






Nonclassical light generation and control from laser-driven semiconductor intraband excitationsIvan Gonoskov ^{1,*}, René Sondenheimer^{2,*}, Christian Hünecke ¹, Daniil Kartashov ³,
Ulf Peschel ⁴ and Stefanie Gräfe ^{1,2,§}¹*Institute of Physical Chemistry, Friedrich Schiller University Jena, Helmholtzweg 4, 07743 Jena, Germany*²*Fraunhofer Institute for Applied Optics and Precision Engineering, Albert-Einstein-Strasse 7, 07745 Jena, Germany*³*Institute of Optics and Quantum Electronics, Friedrich Schiller University Jena, Max-Wien-Platz 1, 07743 Jena, Germany*⁴*Institute of Solid State Theory and Optics, Friedrich Schiller University Jena, Max-Wien-Platz 1, 07743 Jena, Germany*

(Received 21 December 2022; revised 4 November 2023; accepted 8 February 2024; published 7 March 2024)

The generation of higher-order harmonic radiation originating from the interaction of intense laser pulses with matter is typically described semiclassically: While the electronic structure and dynamics of matter is described quantum mechanically, the intense light field is described classically—and accordingly the generated harmonic radiation. However, pioneering experiments on quantum optical properties of high-order harmonic generation (HHG) in atomic gases from the group of P. Tzallas [I. Gonoskov *et al.*, *Sci. Rep.* **6**, 32821 (2016) and N. Tsatrafyllis *et al.*, *Nat. Commun.* **8**, 15170 (2017)], and theoretical investigations from the group of M. Lewenstein [M. Lewenstein *et al.*, *Nat. Phys.* **17**, 1104 (2021) and P. Stammer *et al.*, *Phys. Rev. Lett.* **128**, 123603 (2022)] have impressively demonstrated that light’s quantum properties are observable in the strong-field realm. In this paper, we develop a quantum optical description of HHG in a bulk semiconductor originating from the nonlinear Bloch current. This mechanism of HHG, known as the intraband current, constitutes the major contribution to the emission spectrum for harmonic with energies of quanta roughly below the bandgap. Under certain approximations, employing a quantum description of both light and matter, we obtain analytical solutions, which allow us to analyze the classical and quantum optical characteristics of the fundamental mode of light and the harmonic modes. We find intricate but sufficiently mild modifications of the photon statistics of the fundamental mode and coherent displacements depending on the parameters of the driving laser field. Similar to high-harmonic generation in atoms, the fundamental and emitted harmonic field modes are entangled. Moreover, our analytical model predicts parameter ranges where these quantum optical properties will be most pronounced, allowing protocols for quantum information processing with high photon numbers over a large range of frequencies.

DOI: [10.1103/PhysRevB.109.125110](https://doi.org/10.1103/PhysRevB.109.125110)**I. INTRODUCTION**

An increase of the intensity of a laser, interacting with a gas or solid medium, results in the transition from conventional perturbative nonlinear optics to the realm of strong field phenomena. In particular, nonlinear optical frequency conversion processes, such as the canonical process of (low-order) harmonic generation change towards the emission of nonperturbative, high-order harmonic radiation. In this strong-field regime, depending on the laser parameters (field strength and wavelength), a plateau-like spectrum of the coherent harmonic emission is generated that can span over multiple octaves down to soft x-ray spectral range [1]. Naturally, this emission forms a train of attosecond pulses in the time domain [2]. For atoms (and molecules), the mechanism of HHG can be described via the three-step model of an electron being (1) liberated from the atom by strong-field ionization, (2) its acceleration in the laser field, and (3) its recombination with the

parent ion under emission of the accumulated energy [1,2]. For bulk semiconductors, dielectrics, and nanoscale solids, a similar mechanism has been established [3–10]: (1) Initially, electrons are excited from the system’s valence band (VB) to the conduction band (CB) by the intense laser field, thereby creating a corresponding hole in the conduction band. (2) Subsequently, the electron(s) are (nonlinearly) driven/accelerated in the the conduction band while the hole is driven in the valence band. This nonlinear current gives rise to HHG with energies below the band gap (*intraband mechanism*). (3) The driven electron-hole pair induces a nonlinear polarization (recombination), which leads to the generation of higher harmonics with energies of quanta above the band gap (*interband contribution*). In all cases, the intense driving laser field is considered to be a classical electromagnetic field.

Indeed, these classical theories were very successful in predicting the key features of HHG. Obviously, with high intense laser pulses containing extremely high numbers of photons, quantum corrections are negligible compared to the classical averages [11,12] and a quantum optical treatment of light was considered to be unnecessary. Recently, this paradigm began to shake due to pioneering experiments demonstrating a modification of quantum properties of the emitted high-order harmonic radiation in gases and bulk [13,14]. It raised the

*These authors contributed equally to this work.

†ivan.gonoskov@uni-jena.de

‡rene.sondenheimer@iof.fraunhofer.de

§s.graefe@uni-jena.de

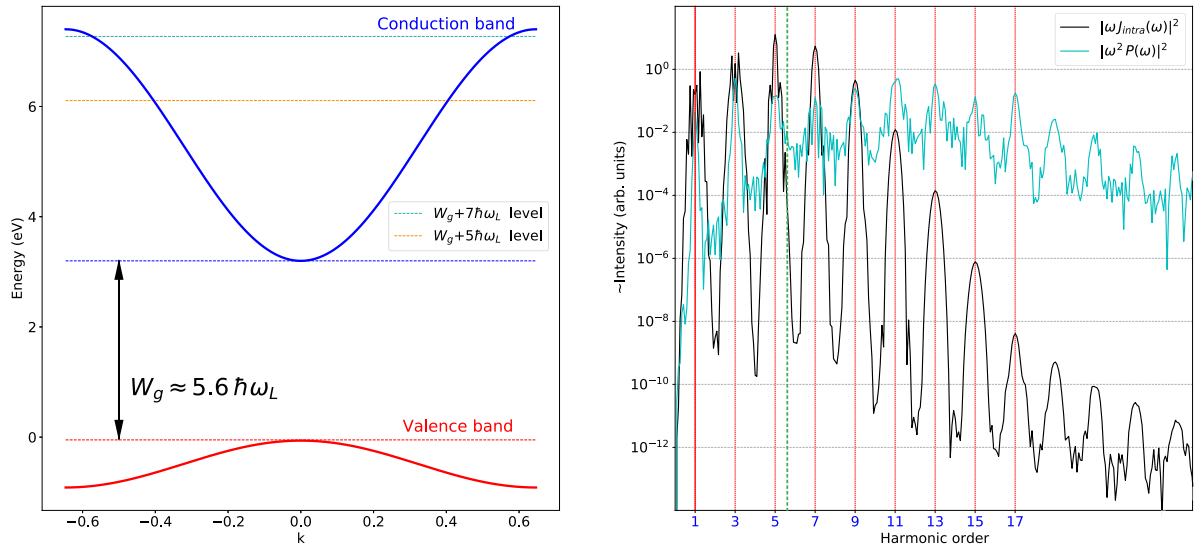


FIG. 1. (Left) Two-band model, with the valence band being parameterized by a cosine potential, see Eq. (7). We consider parameters that correspond to the well-examined zinc oxide (ZnO) [3,14,33]. (Right) Intensity of harmonic emission for both intraband emission J_{intra} and polarization harmonics $P(\omega)$ as a function of Ω/ω_L for the given interaction time (~ 3 optical cycles at FWHM) and the given Bloch parameter $\omega_B/\omega_L = 5.7$ obtained within the SMBE with a dephasing time $T_d = 2.7$ fs. The green vertical line corresponds to the frequency of the bandgap (W_g/\hbar). The intraband current mechanism dominates for the harmonics with energies of quanta below and near the bandgap (i.e., fifth and seventh) by orders of magnitude.

fundamental question to which extent quantum features prevail in nonlinear frequency generation processes involving multiple photons of different frequencies. Moreover, it paves the way towards promising applications such as new measurement techniques [13,14], laser-harmonic and harmonic-harmonic entanglement [15], and the generation of resource states for quantum information processing [16].

However, the theoretical description of a complex quantum system, which includes multiple degrees of freedom faces theoretical challenges and has been only solved for a few special cases [17–20]. For example, very recently, HHG in atoms was considered from a quantum information theory perspective based on positive operator valued measures [21] and allowed for a deeper understanding of potential novel state engineering via HHG [15,16,22–25]. Also, a theoretical description of atomic HHG driven by quantum light has been proposed very recently [26]. One advantage for the analysis of the quantum properties of light produced in HHG in atoms is given by the fact that approximate solutions can be found for the quantum optical states [15,17]. This can be traced back to the fact that the field operator enters the effective interaction Hamiltonian in a linear manner via the dipole approximation [25]. In contrast to the atomic case, for semiconductors, the field operators enter the Hamiltonian in a nonlinear manner according to the band dispersion. So far, there is no quantum optical theoretical description of HHG in the condensed phase.

In this paper, we introduce an analytical quantum optical model of HHG in semiconductors, focusing on the below-bandgap harmonics, i.e., photons generated by *intraband currents*. For IR driving, the role of intraband currents is well understood in terms of the generation of harmonics (for the description of HHG in semiconductors from a semiclassical

perspective see e.g., see [3]). We note parenthetically that also interband polarization contributes to the low-energy side of the harmonic spectrum [27,28]. However, as shown in many papers [4,29], the intraband currents constitute the dominant contribution to lower-order harmonics with photon energies below the band gap of the semiconductor. This will be also the case for the laser parameters investigated in this paper, as we have carefully checked (see also Fig. 1 below).

We here analyze the properties of the generated radiation fields at the classical and quantum level. We propose a model based on an approximate Hamiltonian that captures the relevant mechanism for the intraband harmonics in a fully quantum way.

To illustrate our model, we solve the corresponding time-dependent Schrödinger equation (TDSE) for the combined system comprised of a semiconductor. For the special case of a cosine band structure and quantized light modes, we found analytical solutions. In general, we find non-Gaussian modifications of the radiation field governed by the nonlinear interactions: all field modes are entangled. Our analytical solution allows predicting parameter ranges (in terms of the Bloch frequency) that maximize nonclassical properties. However, these modifications have a rather peculiar structure, such that expectation values of any function of the position quadrature of the pump field are not altered.

The paper is organized as follows: We first introduce the theoretical description of HHG in semiconductors from a quantum perspective and discuss the related approximations and their limitations. We then introduce our analytical method and present approximate analytical solutions assuming a cosine band structure for the conduction band. We compare our analytical solution with a numerical solution obtained from the semiconductor-Maxwell-Bloch equations (SMBE) in the classical regime. Finally, we investigate the nonclassical

properties of the radiation field for higher harmonics described within the intraband mechanism.

II. THEORETICAL MODEL—QUANTUM DESCRIPTION OF HIGHER HARMONICS GENERATED BY INTRABAND CURRENT

We restrict our analysis to a two-band model, as done in many other papers (see, for example, [3,29,30]). Of course, this introduces certain limitations but the (numerical) introduction of further bands is straightforward and would hardly add new physics. In addition, under realistic conditions, mainly the lowest conduction band is significantly populated; thus, motivating our restriction to a two-band model. As we have checked, the dominant intraband mechanism for the considered parameters and harmonics (fifth and seventh) is also valid in more complex calculations, including beyond tight-binding nearest-neighbors approximation and multiband models. We note that for very small energetic separation to higher conduction bands or long driving wavelength towards the THz regime [27], when the momenta of the excited electrons driven in the conduction band may become high, transitions to higher bands cannot be neglected (see, e.g., [4,31]).

Initially, upon laser interaction, the (lowest) conduction band is populated by a number of electrons n_e . Those electrons are assumed to move synchronously in the strong driving field, forming the quasiclassical intraband current (similar as in the classical description [3]). In this case, we can approximate the system by a single-particle Hamiltonian with respect to the Bloch electrons of the system using the conduction band dispersion $E_c(\vec{K})$,

$$\hat{H} = n_e E_c \left(\hat{p} - \sum_j \frac{1}{c} \hat{A}_j \right) + \sum_j \omega_j \hat{N}_j, \quad (1)$$

where $\hat{p} - \sum_j \frac{1}{c} \hat{A}_j$ is the Bloch momentum of a single electron in the band. \hat{A}_j is the vector potential operator of the field mode j (atomic units are employed unless otherwise stated). Further, \hat{p} is the momentum of the identical electrons. The interaction-free part of the quantized electromagnetic field modes j is encoded in the terms $\omega_j \hat{N}_j$, with ω_j the corresponding frequency and \hat{N}_j the photon number operator. The Hamiltonian in Eq. (1) contains the following assumptions: We assume that all electrons with fixed, time-independent density $n_e(t) = n_e = \text{const}$ have the same momentum. This approximation is justified for an optical excitation as electrons are generated mainly at one instance within the half cycle and with almost zero momentum. Second, we employ the dipole approximation and neglect propagation effects (considering a relatively thin crystal). For a first analysis, we also neglect internal losses in the material, as well as further contributions causing decoherences (in accordance with the description within the TDSE). A comprehensive analysis of how such dephasing and damping of the coupled material-radiation system influences the photon statistics is outside the description by the TDSE and, thus, beyond the scope of this paper. Finally, we assume that the depletion of the driving laser field is small.

The considered assumptions allow us to evoke the so-called parametric-connection approximation [18].

These approximations physically mean that we assume the intraband current to be solely generated by the driving field. However, it acts back onto the light field, changing its quantum statistics like a parametric drive. The approximate solution obtained from this method describes the quantum evolution of the light field by treating the intraband-current backreaction as a perturbation.

A. Quantum description of intraband current

Transforming into the interaction picture, the interaction Hamiltonian reads

$$\hat{H} = n_e E_c \left(\hat{p} - \sum_j \frac{1}{c} \hat{A}_j(t) \right), \quad (2)$$

where $\hat{A}_j(t) = \exp(it \omega_j \hat{N}_j) \hat{A}_j \exp(-it \omega_j \hat{N}_j)$ is the transformed field operator. We now apply the parametric-connection approximation, as the effect of the laser-induced current in the conduction band back onto the initial light field is small. In other words, the canonical momentum in the relevant reference frame is mainly determined by the driving radiation field, see the details in [18]. Thus, the momentum spread \hat{p} of the electrons is negligible such that we are able to solve the reduced TDSE (electron states will be averaged out) for the light states separately.

We next consider the evolution of the quantized light modes, evoking the parametric-connection approximation. The wave function of the entire radiation field is denoted with $|G\rangle$, encoding all modes distinguished by the j indices. The corresponding frequency of the laser (L) driving field is ω_L , and the frequencies of the generated higher harmonics are $\omega_j = j\omega_L$. The TDSE for the nonaffected vacuum propagation in the interaction picture is $i\partial_t |G\rangle = 0$. The TDSE, which includes the first-order corrections due to quantum backaction of the intraband current reads (see [18])

$$i\frac{\partial}{\partial t} |G\rangle = n_e E_c \left(- \sum_j \frac{1}{c} \hat{A}_j(t) \right) |G\rangle. \quad (3)$$

For further analysis, we will use a position quadrature representation [11,18]. The position and momentum quadratures of the different field modes are $\hat{Q}_j = \frac{1}{\sqrt{2}}(\hat{a}_j + \hat{a}_j^\dagger)$ and $\hat{P}_j = \frac{1}{\sqrt{2i}}(\hat{a}_j - \hat{a}_j^\dagger)$, respectively. Note that we will highlight the fundamental pump mode ($j = 1$) by subscript L, e.g., $\hat{Q}_1 \equiv \hat{Q}_L$. In the position quadrature representation, we obtain $\hat{a}_j = \frac{1}{\sqrt{2}}(\hat{Q}_j + \frac{\partial}{\partial \hat{Q}_j})$ and $\hat{a}_j^\dagger = \frac{1}{\sqrt{2}}(\hat{Q}_j - \frac{\partial}{\partial \hat{Q}_j})$ for the annihilation and creation operators, respectively.

The vector potential operator for the laser field is $\hat{A}_L(t) = \vec{z} \sqrt{\frac{\pi c^2}{\omega_L V}} [\hat{a}_L e^{-i\omega_L t} + \hat{a}_L^\dagger e^{i\omega_L t}]$, where \vec{z} is the polarization direction and V a quantization volume. Correspondingly, for the harmonic modes j is given by $\hat{A}_j(t) = \vec{z}_j \sqrt{\frac{\pi c^2}{\omega_j V}} [\hat{a}_j e^{-i\omega_j t} + \hat{a}_j^\dagger e^{i\omega_j t}]$.

The initial state of the electromagnetic field is given as a product of a coherent state (fundamental mode) and vacuum

states (harmonic modes up to a cutoff M),

$$|G_0\rangle = |\alpha_L\rangle \bigotimes_j |0_j\rangle, \text{ where } j \in \{2, \dots, M\}. \quad (4)$$

In the position representation, this state can be expressed as

$$G_0(\vec{Q}) = \langle \vec{Q} | G_0 \rangle \\ = C \cdot \exp \left[-\frac{1}{2} (Q_L - e^{i\theta_0} \sqrt{2N_0})^2 \right] \cdot \prod_{j=2}^M e^{-Q_j^2/2},$$

where $\vec{Q} = (Q_L, Q_2, \dots, Q_M)$, $|\vec{Q}\rangle = |Q_L\rangle \bigotimes_{j>1} |Q_j\rangle$. In the above equation, θ_0 is the internal field phase, and $N_0 \gg 1$ is the initial average photon number of the driving laser mode, i.e., $\alpha_L = e^{i\theta_0} \sqrt{N_0}$. Without loss of generality, we choose a reference frame in the optical phase space such that $\theta_0 = 0$ for the initial coherent laser mode. In this case, the related amplitude of the classically described vector potential is $A_0 = \sqrt{\frac{4\pi c^2}{\omega_L V} N_0}$.

Under the assumption that the interaction strength is comparatively weak and the interaction time of the intense laser with the semiconductor is sufficiently short, the intense laser field operator can be considered as a local operator, $\hat{z}_L \hat{A}_L(t) \equiv \hat{A}_L(t) \approx \hat{z}_L \sqrt{\frac{2\pi c^2}{\omega_L V}} \cos(\omega_L t) \hat{Q}_L$. Furthermore, it is convenient to separate the contributions from the fundamental laser mode from the other radiation modes, i.e., we write the z projection of the vector operator for the whole system $\hat{A}(t)$ as

$$\hat{A}(t) = \hat{A}_L(t) + \sum_{j \geq 2} \hat{A}_j(t) \\ = \sqrt{\frac{2\pi c^2}{\omega_L V}} \cos(\omega_L t) \hat{Q}_L \\ + \sum_j \sqrt{\frac{\pi c^2}{\omega_j V}} [\hat{a}_j e^{-i\omega_j t} + \hat{a}_j^\dagger e^{i\omega_j t}]. \quad (5)$$

For the initial field $|G_0\rangle$ [Eq. (4)], the norms of the vector operators from Eq. (5) fulfill the inequality $\|\hat{A}_L\| \gg \|\hat{A}_j\|$, i.e., the pump field dominates the harmonic modes. This allows us to linearize the Hamiltonian in the TDSE (3),

$$i \frac{\partial}{\partial t} |G\rangle = \left[n_c E_c \left(\frac{1}{c} \hat{A}_L(t) \right) + n_c \sum_j \frac{1}{c} \hat{A}_j(t) \cdot \frac{\partial E_c}{\partial \vec{K}} \right]_{K=\frac{1}{c} \hat{A}_L} \\ \times |G\rangle. \quad (6)$$

This is the key equation in this paper. It describes the interaction of light with a semiconductor as driving an intraband in the conduction band with band dispersion $E_c(\vec{k})$ at a fully quantum mechanical level. Since Eq. (6) is linear with respect to $\hat{P}_j = -i\partial_{Q_j}$, it can be solved analytically.

B. Analytical solutions within a cosine band model

To illustrate the power of Eq. (6), we represent the band structure of the conduction band by a cosine, as it was done, e.g., in [3,32]. As shown in [33], such approximation provides appropriate results for lower harmonics. Thus, the conduction

band dispersion is given by

$$E_c(K) = E_g [1 - \cos(\pi K/K_c)], \quad (7)$$

where K_c is the inverse lattice constant, and E_g the conduction band half-width and corresponds to the strength of the orbital interactions within the semiconductor. Using this cosine potential, it is further convenient to use the real-valued Jacobi–Anger expansions with the Bessel functions of the first kind J_k to analyze Eq. (6),

$$\cos[x_1 \cos(x_2)] = J_0(x_1) + 2 \sum_{n=1}^{\infty} (-1)^n J_{2n}(x_1) \cos(2n x_2),$$

$$\sin[x_1 \cos(x_2)] = -2 \sum_{n=1}^{\infty} (-1)^n J_{2n-1}(x_1) \cos((2n-1)x_2).$$

Due to the fact that the commutator of the Hamiltonian of the system with itself at different times is merely proportional to a function depending on time and the quadrature operator \hat{Q}_L , $[\hat{H}(t), \hat{H}(t')] = c(t, t'; \hat{Q}_L)$, all higher-order commutators of the Baker-Campbell-Hausdorff formula vanish when the unitary time-evolution operator is constructed. Thus, the final state is given by

$$|G\rangle = e^{if(t; \hat{Q}_L)} \exp \left\{ \sum_j \alpha_j(t; \hat{Q}_L) a_j^\dagger - [\alpha_j(t; \hat{Q}_L)]^\dagger a_j \right\} |G_0\rangle \quad (8)$$

where

$$f(t; \hat{Q}_L) = n_c E_g [J_0(\gamma_L \hat{Q}_L) - 1] (t - t_0) \\ + 2n_c E_g \sum_{n=1}^{\infty} (-1)^n J_{2n}(\gamma_L \hat{Q}_L) \int_{t_0}^t d\tau \cos(2n \omega_L \tau) \\ + 2n_c^2 E_g^2 \sum_j \sum_{n=1}^{\infty} \sum_{m=1}^{\infty} (-1)^{n+m} \gamma_j^2 \times \int_{t_0}^t d\tau \int_{t_0}^{\tau} d\tau' \\ \times [\cos((2n-1)\omega_L \tau) \cos((2m-1)\omega_L \tau')] \\ \times \sin(\omega_j(\tau' - \tau)) J_{2n-1}(\gamma_L \hat{Q}_L) J_{2m-1}(\gamma_L \hat{Q}_L)$$

with abbreviation $\gamma_{L/j} = \sqrt{2\pi^3/(\omega_{L/j} V K_c^2)}$ and

$$\alpha_j(t; \hat{Q}_L) = i\sqrt{2} n_c E_g \sum_{n=1}^{\infty} (-1)^n \gamma_j J_{2n-1}(\gamma_L \hat{Q}_L) \\ \times \int_{t_0}^t d\tau \cos((2n-1)\omega_L \tau) e^{i\omega_j \tau}. \quad (9)$$

The first exponential in Eq. (8) only contributes to the modification of the driving laser mode. The second exponential function corresponds to the harmonic generation via displacement operators with peaks of odd orders of ω_L following the time integral dependencies in the expression for $\alpha_j(t; \hat{Q}_L)$. The generation of these modes is intertwined with further non-Gaussian modifications of the pump field given by the nonlinear \hat{Q}_L dependencies of the coherent displacements. For the following investigations, it is also useful to study the

solution in Eq. (8) in the position quadrature representation,

$$G = e^{if(t;Q_L)} \prod_j e^{-\frac{1}{2}(\alpha_j(t;Q_L))^2 + i\alpha_j(t;Q_L)} e^{\sqrt{2}\alpha_j(t;Q_L)Q_j} G_0. \quad (10)$$

Thus, the obtained expression clearly connects the quantum properties of light with the semiconductor lattice parameters.

III. INTRABAND HARMONICS—CLASSICAL LIMIT

To analyze and discuss the properties and features of the solution of the TDSE, see Eq. (8) or in position quadrature representation Eq. (10), we first consider the classical field limit for the intense nonperturbed driving laser radiation. Following the standard procedure, we calculate the quantum mechanical expectation values of the operators. Since $\langle \hat{Q}_L \rangle_G = \langle \hat{Q}_L \rangle_{G_0} = \sqrt{2N_0} \gg 1$, we have $\gamma_L \hat{Q}_L \rightarrow \gamma_L \langle \hat{Q}_L \rangle = \frac{\omega_B}{\omega_L}$ where $\omega_B = \frac{A_0}{cK_c} \omega_L$ is the Bloch frequency. Typical values of semiconductor crystals for the ratio ω_B/ω_L are

$$\frac{\omega_B}{\omega_L} = \frac{A_0}{cK_c} \sim \frac{\lambda\sqrt{I_0}}{K_c}, \quad (11)$$

where I_0 is the laser field's peak intensity, $\lambda = \frac{2\pi c}{\omega_L}$ is the driving laser wavelength, and π/K_c is the lattice constant, typically in range of 4–6 Å. For instance, $\omega_B/\omega_L \approx 1$ for $I_0 = 5 \times 10^{11}$ W/cm², $\lambda = 1.44$ μm, and $\pi/K_c = 4.4$ Å (for ZnO, exemplary). In previous experiments, where high harmonic radiation was generated from various semiconductor targets [33,34], a typical ratio is in the range of $\omega_B/\omega_L \leq 5$; although it can be significantly higher when going to mid- or even far-infrared drivers [27].

Using Eq. (10), with these parameters at hand, we calculate the harmonic amplitude ($m = 2n - 1$, and $m \geq 3$),

$$\begin{aligned} E_\Omega \left(\frac{\omega_B}{\omega_L} \right) &= n_e E_g \Omega \sum_m J_m \left(\frac{\omega_B}{\omega_L} \right) \\ &\times \frac{\Omega \sin(\Omega t) \cos(m\omega_L t) - m\omega_L \cos(\Omega t) \sin(m\omega_L t)}{\Omega^2 - m^2\omega_L^2}, \end{aligned} \quad (12)$$

where t is the interaction time of the laser with the semiconductor and Ω is the frequency of the emitted radiation.

In Fig. 2, we compare the emission intensity spectrum obtained from Eq. (12) and from the commonly employed numerical description based on the SMBE (for details, see [35]). The behavior of the odd-harmonic peak intensities coincides very well; however, the background level and harmonic widths differ. These differences can occur because the simplified analytical model does not include a time- and Bloch vector-dependent conduction band population n_e and assumes a monochromatic driving laser field with finite interaction duration t . In addition, the derived analytical solution Eq. (10) of the TDSE of the model Hamiltonian does not include damping effects, as commonly phenomenologically inserted into the SMBE. According to our additional calculations for the different dephasing times (2.7 fs – 10 fs) we found that

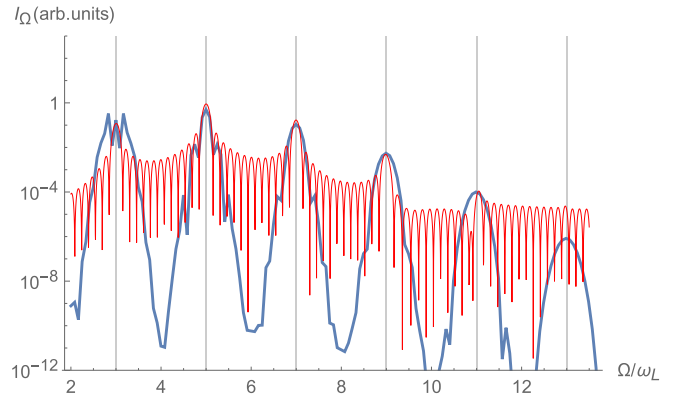


FIG. 2. Intensity of intraband emission as a function of Ω/ω_L for the given interaction time (~ 3 optical cycles at FWHM) and the given Bloch parameter $\omega_B/\omega_L = 5.7$ obtained from our analytical solution (red) and the SMBE (blue). Ω is the frequency of the emitted radiation with clear picks around the higher-order harmonics given by $\Omega = j\omega_L$.

(i) the dephasing time does not at all change the intraband harmonics in the regime that is the focus of our paper. (ii) The polarization-based interband harmonics are increased in magnitude when longer dephasing times are chosen. At the same time, these harmonics become extremely noisy and not well distinguishable for longer dephasing times, as also known from the literature. (iii) Independently of the value of the dephasing time, the intraband current-based contribution to the harmonic spectrum remains by far the dominant part of the harmonic spectrum in the region of interest. As the precise value is not known, we remain with the commonly accepted value of 2.7 fs. We note that we have recently, together with the experiment, identified (momentum-dependent) electron-phonon scattering as the predominant mechanism driving dephasing, and estimated corresponding values [36].

The good agreement of our theoretical approach with the numerical calculations can be utilized in various related applications. For instance, we investigate the dependence of the intensity of a certain intraband harmonic as a function of the laser intensity, using Eq. (12). As an example, we plot the dependence of the intensity of the fifth and seventh harmonic on the driving field's intensity in Fig. 3. We can identify several regions related to the different regimes of the generation (discussed for the fifth harmonic in the following): (1) perturbative regime, for $I_0 \lesssim 10^{11}$ W/cm²; (2) Linear growth with the fastest rate around $I_0 \sim 1 \times 10^{12}$ W/cm²; (3) the first local maximum at $I_0 \sim 1.5 \times 10^{12}$ W/cm², (4) linear decay; and (5) the first local minimum around 3.2×10^{12} W/cm² etc. We consider these regimes in the context of the nonclassical features of the output radiation after the interaction in what follows.

IV. NONCLASSICAL PROPERTIES OF EMITTED RADIATION

For an explorative discussion concerning the nonclassical features of the emitted radiation, we focus on two features: (i) noncoherent modification of the transmitted IR laser, when the related output state of the fundamental mode is not a coherent

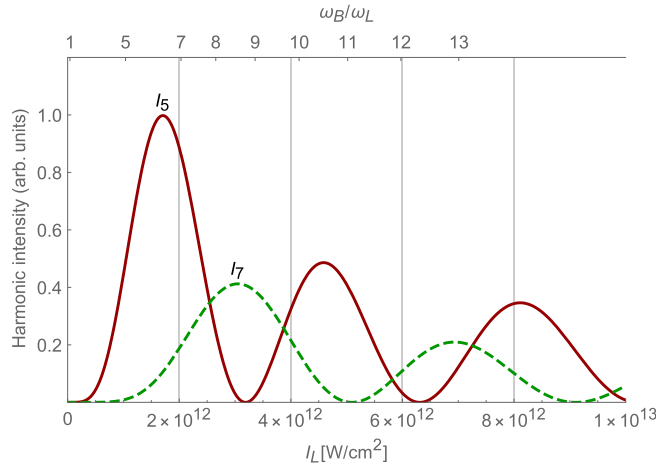


FIG. 3. Intensity of the fifth and seventh harmonic as a function of the laser intensity for $\lambda = 5 \mu\text{m}$ and $\pi/K_c = 4.4 \text{ \AA}$.

state, $\exp(-\frac{1}{2}(\hat{Q}_L - \sqrt{2}\alpha_L)^2)$ and (ii) entanglement between the different modes, i.e., when the state cannot be written as a product state, $G(\vec{Q}) \neq G_L(Q_L) \prod_j G_j(Q_j)$, see also [37].

First of all, the intricate (unitary) time evolution generates non-Gaussian modifications of the fundamental mode according to the nonquadratic dependency on \hat{Q}_L . This is in contrast to HHG in atoms, where a depletion of the pump mode is observed but it remains a coherent state [21,22]. This can be traced back to the fact that the interaction Hamiltonian depends linearly on the field operator resulting in a multimode displacement operator. In our case, the nonlinear band dispersion allows for more involved properties due to nonlinear interactions between the modes. For instance, the unitary operator in Eq. (8) has the structure of a \hat{Q}_L -dependent displacement operator for the harmonics. Additionally, the pump field is altered according to a nontrivial \hat{Q}_L -dependent phase term.

Based on the assumption that the driving laser field is strong and negligibly perturbed, from Eq. (10) we directly obtain that the average of \hat{Q}_L remains unchanged, $\langle \hat{Q}_L \rangle_G = \sqrt{2N_0}$, within our approximations. In particular, this holds for the expectation value of any function of \hat{Q}_L , $\langle f(\hat{Q}_L) \rangle_G = \langle f(\hat{Q}_L) \rangle_{G_0}$. Nevertheless, other expectation values might be altered.

To analyze the quantum properties of the final state $|G\rangle$, we expand the Bessel functions $J_k(\alpha)$ in Eq. (10). Based on the regimes considered in the previous section, we can identify various situations depending on the ratio ω_B/ω_L : For instance, for $\frac{\omega_B}{\omega_L} \ll 1$ (1), we are in the well-known perturbative regime when $I_0 \sim I_{0L}^{2n+1}$ since $J_{2n+1}(\gamma_L Q_L) \sim (\gamma_L Q_L)^{2n+1}$ for $\gamma_L Q_L = \frac{\omega_B}{\sqrt{2N_0}\omega_L} Q_L \ll 1$. In this case, the non-Gaussian modifications of the transmitted IR laser due to the excited intraband current are very small, the field state is almost unaffected and remains almost a coherent state. We note, however, that in this particular regime neglected higher-order terms in the expansion done in Eq. (6) may become dominant compared to the linear term in the harmonic modes. This would then alter the photon statistics of the harmonic modes.

In the second region with the fastest linear growth (2), we can linearize the solution Eq. (10) around $Q_L \approx \sqrt{2N_0}$ and

obtain the following linear approximation of the final state:

$$G \sim G_0(\vec{Q}) e^{\delta_3 Q_1 Q_3} e^{\delta_5 Q_1 Q_5} \dots,$$

with constants δ_j depending on the system's parameters. In this regime, the complex parameters characterizing the displacement of the harmonics are directly proportional to the position quadrature of the pump field $\alpha_j \sim \gamma_j Q_L$: the mean photon number of the harmonics N_j scales proportional to the mean photon number N_0 of the pump laser. Of course, HHG is an inherent nonlinear process inducing a nonlinear relation between the mean photon number of the higher harmonics and the intensity of the pump mode stored in the parameter α_L , $\langle \hat{N}_j \rangle \sim \int dQ_L |\alpha_j(t; Q_L)|^2 e^{-(Q_L - \sqrt{2}\alpha_L)^2}$. However, the nonlinear properties become subleading in this particular regime cf. Fig. 3. Additionally, we obtain slight deviations for the exception value of the momentum quadrature \hat{P}_L compared to the initial state $|G_0\rangle$. However, these deviations are sufficiently small. In particular, we have $\langle \hat{P}_L \rangle_G = -\frac{1}{2} n_e E_g \frac{\omega_B^2}{\sqrt{2N_0}\omega_L^2} t$ at lowest order in the interaction time t , the energy of the intraband current $\sim n_e E_g$, and the dimensionless Bloch parameter $\frac{\omega_B}{\omega_L}$.

To investigate potential entanglement between the different frequency modes, we have to perform a conditioning on the generation of harmonic modes. Such a conditioning can be performed by the projection operator $\hat{\mathbf{I}} - |G_0\rangle\langle G_0|$ [21]. Its orthogonal complement $|G_0\rangle\langle G_0|$ projects on the subspace where no harmonic radiation has been generated via the process. In case higher harmonic modes are excited, which is trivially heralded by the emission of harmonic radiation, the correspondingly projected state is given by

$$\begin{aligned} |G_{\text{HHG}}\rangle &= (\hat{\mathbf{I}} - |G_0\rangle\langle G_0|) |G\rangle = |G\rangle - |G_0\rangle\langle G_0| |G\rangle \\ &= |G\rangle - \langle \alpha_L | e^{if(t, \hat{Q}_L) - \frac{1}{2} \sum_j \alpha_j^\dagger(t, \hat{Q}_L) \alpha_j(t, \hat{Q}_L)} | \alpha_L \rangle | G_0 \rangle. \end{aligned} \quad (13)$$

Note that this conditioning is necessary as the initial and final state have nontrivial overlap $\langle G_0 | G \rangle \neq 0$ as the coherent states form an overcomplete basis and, thus, are not orthogonal in general. This also implies that the resulting state conditioned on HHG $|G_{\text{HHG}}\rangle$ is massively entangled between all optical modes, which can again be conveniently explored in the position representation

$$\begin{aligned} \langle \vec{Q} | G_{\text{HHG}} \rangle &= \langle \vec{Q} | e^{if(t; Q_L)} | \alpha_L \rangle \otimes_j | \alpha_j(t; Q_L) \rangle \\ &= \langle \vec{Q} | \int dQ_L e^{if(t; Q_L)} |\langle Q_L | \alpha_L \rangle|^2 | \alpha_L \rangle \otimes_j | 0_j \rangle. \end{aligned} \quad (14)$$

Equation (14) clearly demonstrates that the state conditioned on HHG cannot be written as a simple product of wave functions and is nonseparable. Therefore, the generation of higher harmonics via the interaction of the pump field with the nonlinear intraband structure of a semiconductor naturally produces an entanglement between all present field modes. In our specific case, the entangled state $\langle \vec{Q} | G_{\text{HHG}} \rangle$ is on structural grounds similar to the entangled state produced in HHG in atoms [23] or recently in solids within a Wannier-Bloch picture [38].

In general, it is not surprising that a highly nonlinear process as HHG produces entanglement. But, apart from the

different modification of the pump field, the higher-order harmonics allow for a multipartite entangled coherent state. Such states can provide a powerful resource for general quantum information processing [39], e.g., for improved phase estimation [40], violations of Bell inequalities for continuous variables [41], and quantum state engineering [42]. The main advantage of the HHG process is that harmonics can be produced over a broad spectral range from infrared to ultraviolet. The complex numbers α_j characterizing the displacements generally depend in a nonlinear way on the position quadrature of the fundamental mode allowing for large photon numbers in the harmonic modes. Already in the regime dominated by the minimum of the intraband potential, we obtain $|\alpha_j|^2 \sim N_0$. Of course our analytical approach only provides a first evidence. Based on our analytical results, further investigations will allow to quantify the degree of entanglement.

V. SUMMARY AND CONCLUSIONS

To summarize, we have provided an analytical theory to describe the quantum optical properties of high-order harmonic generation (HHG) in a bulk semiconductor. We have focused on the lower part of harmonics with energies of quanta below the semiconductor's bandgap, which are mechanically dominated by a nonlinear intraband current in the conduction band, driven by the intense laser field. Under the assumption that the effect of the induced current back on the initial laser field is small (parametric-connection approximation), we have derived equations describing the evolution of multimode light-induced intraband excitations within a full quantum description.

Within a first-order approximation, we have analyzed classical and nonclassical properties of the emitted radiation.

In particular, HHG in semiconductors leads to entanglement between all optical modes in a natural way. On structural grounds, this is similar to HHG in atoms. A crucial difference arises due to the stronger dependence of the harmonics on the properties of the fundamental mode due to nonlinear back-interactions induced via the band dispersion. We showed that nonclassical effects like harmonic entanglement or noncoherent driving-laser state correction could arise. The analytical model allows identifying the key parameter responsible for the nonclassicality and discussing specific regions where the considered nonclassical features may become most pronounced. Further extension of the model to the second-order approximation analog of the Eq. (6) could demonstrate the generation of harmonics with noncoherent wavefunction and possible harmonic-harmonic entanglement.

In future studies, further contributions need to be addressed and taken into account, including the impact of the restriction to a single band, field depletion, dephasing, and etc. Our results and subsequent studies might open possibilities for the engineering of complex photonic resource states for quantum information processing.

ACKNOWLEDGMENTS

I.G., C.H., D.K., U.P., and S.G. acknowledge funding by Q-Hub Thüringen and the German Science Foundation DFG via SFB 1375 NOA (Project No. 398816777), Projects A1 and C4. S.G. and I.G. also acknowledge funding from the ERC Consolidator grant QUEM-CHEM Project No. 772676. R.S. acknowledges funding by the European Union's Horizon 2020 Research and Innovation Action under Grant Agreement No. 899824 (SURQUID) and valuable discussions with Gregor Sauer and Fabian Steinlechner.

-
- [1] P. B. Corkum, Plasma perspective on strong field multiphoton ionization, *Phys. Rev. Lett.* **71**, 1994 (1993).
 - [2] P. B. Corkum and F. Krausz, Attosecond science, *Nat. Phys.* **3**, 381 (2007).
 - [3] D. Golde, T. Meier, and S. W. Koch, High harmonics generated in semiconductor nanostructures by the coupled dynamics of optical inter- and intraband excitations, *Phys. Rev. B* **77**, 075330 (2008).
 - [4] L. Yue and M. B. Gaarde, Introduction to theory of high-harmonic generation in solids: Tutorial, *J. Opt. Soc. Am. B* **39**, 535 (2022).
 - [5] U. Peschel, M. Thümmler, T. Lettau, S. Gräfe, and K. Busch, Two-particle tight-binding description of higher-harmonic generation in semiconductor nanostructures, *Phys. Rev. B* **106**, 245307 (2022).
 - [6] H. N. Gopalakrishna, R. Baruah, C. Hünecke, V. Korolev, M. Thümmler, A. Croy, M. Richter, F. Yahyaei, R. Hollinger, V. Shumakova, I. Uschmann, H. Marschner, M. Zürich, C. Reichardt, A. Undisz, J. Dellith, A. Pugžlys, A. Baltuška, C. Spielmann, U. Peschel *et al.*, Tracing spatial confinement in semiconductor quantum dots by high-order harmonic generation, *Phys. Rev. Res.* **5**, 013128 (2023).
 - [7] C. Heide, Y. Kobayashi, A. C. Johnson, T. F. Heinz, D. A. Reis, F. Liu, and S. Ghimire, High-harmonic generation from artificially stacked 2D crystals, *Nanophotonics* **12**, 255 (2023).
 - [8] K. Nakagawa, H. Hirori, S. A. Sato, H. Tahara, F. Sekiguchi, G. Yumoto, M. Saruyama, R. Sato, T. Teranishi, and Y. Kanemitsu, Size-controlled quantum dots reveal the impact of intraband transitions on high-order harmonic generation in solids, *Nat. Phys.* **18**, 874 (2022).
 - [9] T. T. Luu, M. Garg, S. Yu Kruchinin, A. Moulet, M. Th. Hassan, and E. Goulielmaki, Extreme ultraviolet high-harmonic spectroscopy of solids, *Nature (London)* **521**, 498 (2015).
 - [10] G. Vampa, T. J. Hammond, M. Taucer, X. Ding, X. Ropagnol, T. Ozaki, S. Delprat, M. Chaker, N. Thiré, B. E. Schmidt, F. Légaré, D. D. Klug, A. Yu. Naumov, D. M. Villeneuve, A. Staudte, and P. B. Corkum, Strong-field optoelectronics in solids, *Nat. Photon.* **12**, 465 (2018).
 - [11] L. Mandel and E. Wolf, *Optical Coherence and Quantum Optics* (Cambridge University Press, Cambridge, 1995).
 - [12] H. Spohn, *Dynamics of Charged Particles and Their Radiation Field* (Cambridge University Press, Cambridge, 2004).
 - [13] N. Tsatrafyllis, I. K. Kominis, I. A. Gonoskov, and P. Tzallas, High-order harmonics measured by the photon statistics of the infrared driving-field exiting the atomic medium, *Nat. Commun.* **8**, 15170 (2017).

- [14] N. Tsatrafyllis, S. Kühn, M. Dumergue, P. Foldi, S. Kahaly, E. Cormier, I. A. Gonoskov, B. Kiss, K. Varju, S. Varro, and P. Tzallas, Quantum optical signatures in a strong laser pulse after interaction with semiconductors, *Phys. Rev. Lett.* **122**, 193602 (2019).
- [15] P. Stammer, J. Rivera-Dean, T. Lamprou, E. Pisanty, M. F. Ciappina, P. Tzallas, and M. Lewenstein, High photon number entangled states and coherent state superposition from the extreme ultraviolet to the far infrared, *Phys. Rev. Lett.* **128**, 123603 (2022).
- [16] M. Lewenstein, M. F. Ciappina, E. Pisanty, J. Rivera-Dean, P. Stammer, Th. Lamprou, and P. Tzallas, Generation of optical Schrödinger cat states in intense laser-matter interactions, *Nat. Phys.* **17**, 1104 (2021).
- [17] I. A. Gonoskov, N. Tsatrafyllis, I. K. Kominis, and P. Tzallas, Quantum optical signatures in strong-field laser physics: Infrared photon counting in high-order-harmonic generation, *Sci. Rep.* **6**, 32821 (2016).
- [18] I. Gonoskov and S. Gräfe, Light-matter quantum dynamics of complex laser-driven systems, *J. Chem. Phys.* **154**, 234106 (2021).
- [19] D. N. Makarov, Quantum theory of scattering of ultrashort electromagnetic field pulses by polyatomic structures, *Opt. Express* **27**, 31989 (2019).
- [20] P. Földi, I. Magashegyi, Á. Gombkőto, and S. Varró, Describing high-order harmonic generation using quantum optical models, *Photonics* **8**, 263 (2021).
- [21] P. Stammer, Theory of entanglement and measurement in high-order harmonic generation, *Phys. Rev. A* **106**, L050402 (2022).
- [22] M. Lewenstein, N. Baldelli, U. Bhattacharya, J. Biegert, M. F. Ciappina, U. Elu, T. Grass, P. T. Grochowski, A. Johnson, T. Lamprou, A. S. Maxwell, A. Ordóñez, E. Pisanty, J. Rivera-Dean, P. Stammer, I. Tyulnev, and P. Tzallas, Attosecond physics and quantum information science, [arXiv:2208.14769](https://arxiv.org/abs/2208.14769).
- [23] P. Stammer, J. Rivera-Dean, A. Maxwell, T. Lamprou, A. Ordóñez, M. F. Ciappina, P. Tzallas, and M. Lewenstein, Quantum electrodynamics of ultra-intense laser-matter interactions, *PRX Quantum* **4**, 010201 (2023).
- [24] A. Pizzi, A. Gorlach, N. Rivera, A. Nunnenkamp, and I. Kaminer, Light emission from strongly driven many-body systems, *Nat. Phys.* **19**, 551 (2023).
- [25] J. Rivera-Dean, Th. Lamprou, E. Pisanty, P. Stammer, A. F. Ordóñez, A. S. Maxwell, M. F. Ciappina, M. Lewenstein, and P. Tzallas, Strong laser fields and their power to generate controllable high-photon-number coherent-state superpositions, *Phys. Rev. A* **105**, 033714 (2022).
- [26] A. Gorlach, M. E. Tzur, M. Birk, M. Krüger, N. Rivera, O. Cohen, and I. Kaminer, High-harmonic generation driven by quantum light, *Nat. Phys.* **19**, 1689 (2023).
- [27] O. Schubert, M. Hohenleutner, F. Langer, B. Urbanek, C. Lange, U. Huttner, D. Golde, T. Meier, M. Kira, S. W. Koch, and R. Huber, Sub-cycle control of terahertz high-harmonic generation by dynamical Bloch oscillations, *Nat. Photon.* **8**, 119 (2014).
- [28] A. Chacón, D. Kim, W. Zhu, S. P. Kelly, A. Dauphin, E. Pisanty, A. S. Maxwell, A. Picón, M. F. Ciappina, D. E. Kim, C. Ticknor, A. Saxena, and M. Lewenstein, Circular dichroism in higher-order harmonic generation: Heralding topological phases and transitions in Chern insulators, *Phys. Rev. B* **102**, 134115 (2020).
- [29] G. Vampa, C. R. McDonald, G. Orlando, D. D. Klug, P. B. Corkum, and T. Brabec, Theoretical analysis of high-harmonic generation in solids, *Phys. Rev. Lett.* **113**, 073901 (2014).
- [30] M. Sheik-Bahae, D. C. Hutchings, D. J. Hagan, and E. W. Van Stryland, Dispersion of bound electron nonlinear refraction in solids, *IEEE J. Quantum Electron.* **27**, 1296 (1991).
- [31] P. G. Hawkins, M. Yu. Ivanov, and V. S. Yakovlev, Effect of multiple conduction bands on high-harmonic emission from dielectrics, *Phys. Rev. A* **91**, 013405 (2015).
- [32] S. Ghimire, A. D. DiChiara, E. Sistrunk, G. Ndabashimiye, U. B. Szafruga, A. Mohammad, P. Agostini, L. F. DiMauro, and D. A. Reis, Generation and propagation of high-order harmonics in crystals, *Phys. Rev. A* **85**, 043836 (2012).
- [33] S. Ghimire, A. D. DiChiara, E. Sistrunk, P. Agostini, L. F. DiMauro, and D. A. Reis, Observation of high-order harmonic generation in a bulk crystal, *Nat. Phys.* **7**, 138 (2011).
- [34] N. Yoshikawa, K. Nagai, K. Uchida, Y. Takaguchi, S. Sasaki, Y. Miyata, and K. Tanaka, Interband resonant high-harmonic generation by valley polarized electron-hole pairs, *Nat. Commun.* **10**, 3709 (2019).
- [35] C. Yu, S. Jiang, and R. Lu, High order harmonic generation in solids: A review on recent numerical methods, *Adv. Phys.: X* **4**, 1562982 (2019).
- [36] V. Korolev, T. Lettau, V. Krishna, A. Croy, M. Zuerch, C. Spielmann, M. Waechtler, U. Peschel, S. Graefe, G. Soavi, and D. Kartashov, Unveiling the role of electron-phonon scattering in dephasing high-order harmonics in solids, [arXiv:2401.12929](https://arxiv.org/abs/2401.12929).
- [37] O. Gühne and G. Tóth, Entanglement detection, *Phys. Rep.* **474**, 1 (2009).
- [38] J. Rivera-Dean, P. Stammer, A. S. Maxwell, T. Lamprou, A. F. Ordóñez, E. Pisanty, P. Tzallas, M. Lewenstein, and M. F. Ciappina, Quantum optical analysis of high-harmonic generation in solids within a Wannier-Bloch picture, [arXiv:2211.00033](https://arxiv.org/abs/2211.00033).
- [39] H. Jeong, M. S. Kim, and J. Lee, Quantum-information processing for a coherent superposition state via a mixed-entangled coherent channel, *Phys. Rev. A* **64**, 052308 (2001).
- [40] J. Joo, W. J. Munro, and T. P. Spiller, Quantum metrology with entangled coherent states, *Phys. Rev. Lett.* **107**, 083601 (2011).
- [41] A. Gilchrist, P. Deuar, and M. D. Reid, Contradiction of quantum mechanics with local hidden variables for quadrature phase measurements on pair-coherent states and squeezed macroscopic superpositions of coherent states, *Phys. Rev. A* **60**, 4259 (1999).
- [42] I. A. Walmsley, Quantum optics: Science and technology in a new light, *Science* **348**, 525 (2015).